Analyses of Metro Train-Induced Vibration of Building Above Subway Tunnel

Jianjin Yang, Wanming Zhai, Shengyang Zhu and Yu Guo

Abstract To more accurately predict the structural vibration of the building above the subway tunnel due to the train moving on the floating-slab track (FST), a prediction model is established in this paper. The model is developed based on the vehicle-track coupled dynamics and is comprised of two subsystems. The first subsystem is the spatial train-FST coupled dynamic subsystem and the second subsystem is the FST-tunnel-soil-building coupled dynamic subsystem. The relationship between the two subsystems is the dynamic reaction forces supporting the rails. In the first subsystem, the train is marshalled by several vehicles and each vehicle is simplified as multi-rigid-body system with 35 DOFs. In the second subsystem, the subway tunnel, the building above the tunnel and the soil around the tunnel are modelled using finite elements, and the 3D consistent viscous-spring artificial boundaries are applied to mitigate the impact of artificial boundaries on the calculation results.

Keywords Building vibration · Subway tunnel · Moving train · Vehicle–track coupled dynamics

1 Introduction

In China, there are many cities in the plan and construction of urban rail transit, and the scale of construction is the biggest in the world [1]. In order to provide a more convenient, more highly effective and faster mean of transportation, the subway is getting closer and closer to the building where people live and even the subway and the building are built together. Unfortunately, this will aggravate the vibration of the building induced by the running train, which has quite adverse influences on the structural safety of the buildings, the operating of precision instruments and the life quality of residents in the building. This paper focuses on the structural vibration of

J. Yang (✉) · W. Zhai · S. Zhu · Y. Guo
State Key Laboratory of Traction Power, Southwest Jiaotong University, Chengdu, China
e-mail: jjyang007@hotmail.com

E. Tutumluer et al. (eds.), *Advances in Environmental Vibration and Transportation Geodynamics*, Lecture Notes in Civil Engineering 66,
https://doi.org/10.1007/978-981-15-2349-6_41

a hotel induced by the running train. The hotel is built above the subway tunnel and their structures are built together and the tunnel is built for two roads and two metro lines of FST, illustrated in Fig. 1.

The prediction of the building vibration induced by the moving train belongs to the environmental vibration induced by railway transportation, which is a comprehensive multi-disciplined engineering problem involving the multi-body dynamics, the structural dynamics, the soil dynamics and the train-track coupled dynamic interaction. There are many methods to predict the environmental vibration induced by railway transportation, such as the two-dimensional (2D) methodology [2, 3], two-and-half-dimensional (2.5D) methodology [4–8], pipe-in-pipe (PiP) method [9] and the formulation of periodic structure [10]. These methods, which are based on some hypotheses and simplifications, have high computational speed but low applicability to the problems involving complicated geometries and structures. Besides, these methods adopt the linear wheel/rail interaction, so they cannot veritably reflect the influence of train on the ground vibration; however, the train plays an important role in the moving train-induced environment vibration [11]. To more accurately predict the structural vibration of the hotel with complicated geometry and structure, a model consisting of the spatial train-FST coupled dynamic subsystem and the FST–tunnel–soil–building coupled dynamic subsystem is developed based on the vehicle–track coupled dynamics [12–15].

In the first subsystem, the spatial train–FST coupled dynamics model is used to calculate the dynamic reaction forces supporting the rails (abbreviated as fastener forces). In the spatial train–FST dynamic interaction model, the dynamic wheel/rail interaction model [16] is adopted and the geometric irregularities of wheels and rails are taken as the excitation. In this subsystem, the influence of the deformations of the track base is ignored. In fact, the influence of the deformations of the track base on the fastener forces is quite small.

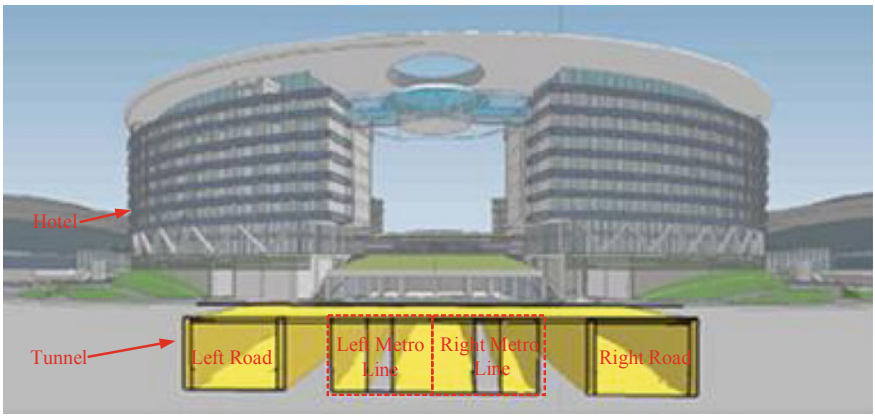

Fig. 1 Position relation between the hotel and the tunnel

In the second subsystem, the FST, the tunnel, the soil and the building are elaborately modelled using the finite element (FE) method, and are coupled through the deformation compatibility conditions at the interfaces to form a FE dynamics model of track–tunnel–soil–building system. In this subsystem, the complicated geometry of the building and the layering of the soil are fully considered in the FE model.

It can be found that these two subsystems are correlated by the fastener forces. This correlation method has also been used in our previous works [17, 18] and Kouroussis' work [19].

2 Prediction Model

2.1 *Spatial Train–FST Coupled Dynamics Subsystem*

A metro train is marshalled by a series of vehicles with the similar main components, one car body, two bogie frames, four wheelsets and two stages of suspensions. When a metro train moves on the FST, it will induce the vibration of the track which can be in reverse influence the dynamic behaviors of the vehicle. Obviously, the vehicle and the FST are essentially coupled with each other. Based on the theory of vehicle–track coupled dynamics [12–15], the spatial train–FST coupled dynamics model is established, as illustrated in Fig. 2.

As the basic unit of the metro train, the vehicle is modelled as a four-axle mass-spring-damper system of 35 degrees of freedom (DOFs), listed in Table 1. By using the system of coordinates moving along the track with vehicle speed, the equations of motion of the vehicle subsystem can be easily derived according to the D'Alembert's principle, which can be described in the form of second-order differential equations in the time domain:

$$\mathbf{M}_{\mathrm{V}}\mathbf{A}_{\mathrm{V}} + \mathbf{C}_{\mathrm{V}}(\mathbf{V}_{\mathrm{V}})\mathbf{V}_{\mathrm{V}} + \mathbf{K}_{\mathrm{V}}(\mathbf{X}_{\mathrm{V}})\mathbf{X}_{\mathrm{V}} = \mathbf{F}_{\mathrm{V}}(\mathbf{X}_{\mathrm{V}}, \mathbf{V}_{\mathrm{V}}, \mathbf{X}_{\mathrm{T}}, \mathbf{V}_{\mathrm{T}}) + \mathbf{F}_{\mathrm{EXT}} \quad (1)$$

where $\mathbf{X}_{\mathrm{V}}$, $\mathbf{V}_{\mathrm{V}}$ and $\mathbf{A}_{\mathrm{V}}$ are the vectors of displacements, velocities and accelerations of the vehicle subsystem, respectively; $\mathbf{M}_{\mathrm{V}}$ is the mass matrix of the vehicle which is a 35×35 diagonal matrix; $\mathbf{C}_{\mathrm{V}}(\mathbf{V}_{\mathrm{V}})$ and $\mathbf{K}_{\mathrm{V}}(\mathbf{X}_{\mathrm{V}})$ are the damping and the stiffness matrices to describe the nonlinearities within the suspensions at the current state of the vehicle subsystem; $\mathbf{X}_{\mathrm{T}}$ and $\mathbf{V}_{\mathrm{T}}$ are the vectors of displacements and velocities of the track subsystem; $\mathbf{F}_{\mathrm{V}}(\mathbf{X}_{\mathrm{V}},\mathbf{V}_{\mathrm{V}},\mathbf{X}_{\mathrm{T}},\mathbf{V}_{\mathrm{T}})$ is the load vector representing the nonlinear wheel/rail contact forces determined by the dynamic wheel/rail coupled model, which depend on the motions $\mathbf{X}_{\mathrm{V}}$ and $\mathbf{V}_{\mathrm{V}}$ of the vehicle and $\mathbf{X}_{\mathrm{T}}$ and $\mathbf{V}_{\mathrm{T}}$ of the track; and $\mathbf{F}_{\mathrm{EXT}}$ describes the external forces including gravitational forces and forces resulting from the centripetal acceleration when the vehicle is running through a curve. The details of the vehicle subsystem dynamic model refer to [12–15].

For the vertical, lateral and torsional vibration, the rail can be simplified as a simply supported beam due to its large ratio of length to cross section.

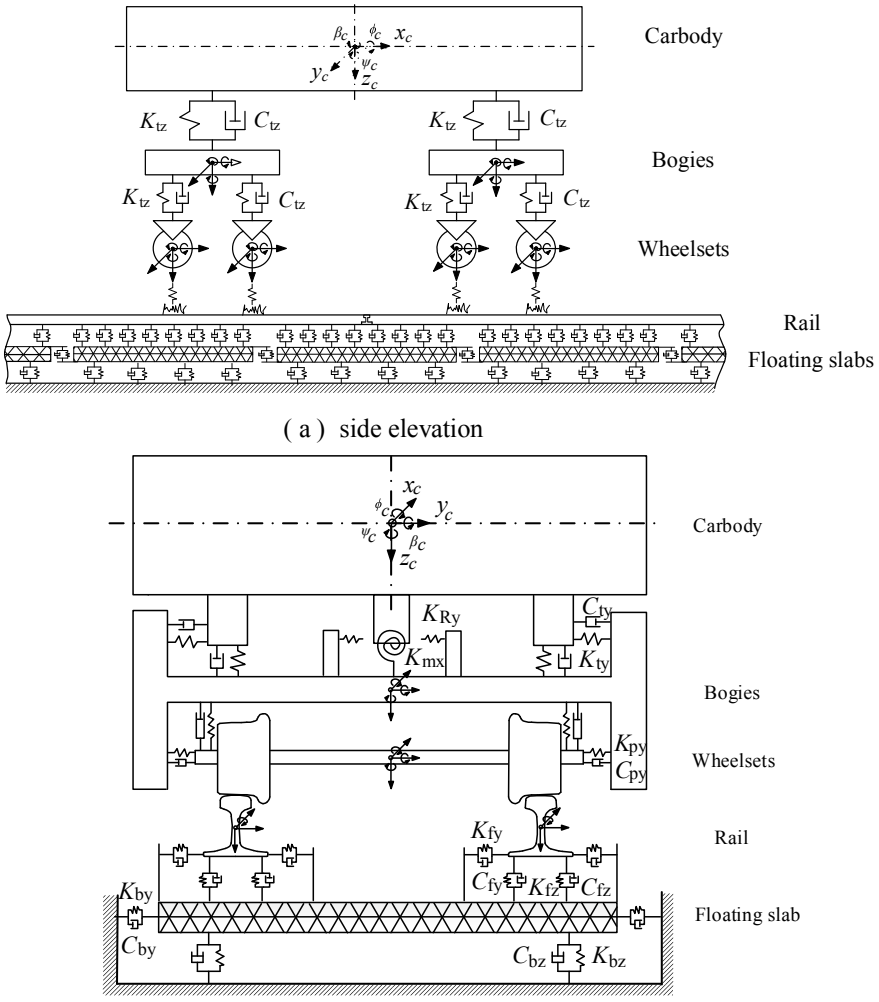

Fig. 2 Spatial vehicle–FST coupled dynamic model

The equations of motion of the rail are given in the form of the fourth-order partial differential equations.

Described by a thin plate supported by slab bearings on rigid foundation, the vertical displacements of the *k*th floating slab can be written in form of the fourth-order partial differential equations in the time domain. For both the lateral vibration and the rotation in the horizontal plane, the floating slab can be treated as rigid body.

Both the fasteners and slab bearings are modelled as ordinary Kelvin elements. The elastic restoring forces of the fastener are proportional to the relative

Table 1 DOFs of a vehicle

Vehicle component	Lateral motion	Vertical motion	Roll motion	Yaw motion	Pitch motion
Car body	y_c	z_c	ϕ_c	ψ_c	β_c
Bogie frame 1	y_{t1}	z_{t1}	ϕ_{t1}	ψ_{t1}	β_{t1}
Bogie frame 2	y_{t2}	z_{t2}	ϕ_{t2}	ψ_{t2}	β_{t2}
Wheelset 1	y_{w1}	z_{w1}	ϕ_{w1}	ψ_{w1}	β_{w1}
Wheelset 2	y_{w2}	z_{w2}	ϕ_{w2}	ψ_{w2}	β_{w2}
Wheelset 3	y_{w3}	z_{w3}	ϕ_{w3}	ψ_{w3}	β_{w3}
Wheelset 4	y_{w4}	z_{w4}	ϕ_{w4}	ψ_{w4}	β_{w4}

displacements and relative velocities between the rail and the floating slab at the ends of the fastener, and the supporting forces of the slab bearing are proportional to the displacements and velocities of the floating slab at the position of the slab bearing.

As described above, the equations of motion of the FST involve second- and fourth-order partial differential equations. To facilitate solution procedure, all partial differential equations are transformed into a series of second-order ordinary differential equations by means of Ritz's method, and then the time-stepping integration method is adopted. The transformation results could be found in references [12–15]. The final equations of the FST could also be assembled into the standard matrix form, similar to Eq. (1), as

$$\mathbf{M}_T\mathbf{A}_T + \mathbf{C}_T\mathbf{V}_T + \mathbf{K}_T\mathbf{X}_T = \mathbf{F}_T(\mathbf{X}_V, \mathbf{V}_V, \mathbf{X}_T, \mathbf{V}_T) \tag{2}$$

where $\mathbf{M}_T$, $\mathbf{C}_T$ and $\mathbf{K}_T$ are the mass, damping and the stiffness matrix of the track, respectively, and $\mathbf{F}_T$ is the load vector of the track model representing the wheel/rail forces obtained by the dynamic wheel/rail coupled model.

The vehicle and the track interact with each other through the dynamic wheel/rail interaction, which will be described using the dynamic wheel/rail coupled model [16]. In the dynamic wheel/rail coupled model, three kinds of rail motions in vertical, lateral and torsional directions are taken into account.

The vehicle-track coupled vibrations are mainly excited by the random track irregularities which are usually expressed by a one-sided power spectrum density (PSD) function, namely track spectrum. The sixth grade track irregularity PSD of US railways is long wave track irregularity of more than 1.0 m wave length and is usually used as the excitation to analyze the vibration in low frequency range which is usually not more than 100 Hz. In this paper, in order to analyze the building vibration in wider frequency range, Sato spectrum of the short wave track irregularity of 0.05–1.0 m wave length is used, which is expressed as

$$S(f) = Af^{-n} \tag{3}$$

where the unit of $S(f)$ is $mm^2/(1/m)$; $f = 1/\lambda$ is the spatial frequency in cycle/m; A and n are the fit coefficients.

A fast and high-precision numerical transformation method [20] is adopted to transform the PSD function of the track spectrum into the time-domain random track irregularity. Figures 3 and 4 illustrate the transformed time-domain random track irregularity.

The spatial train-FST coupled dynamics system is a large-scale nonlinear coupled dynamic system. To efficiently solve the nonlinear dynamic system of such high DOFs, the Zhai method, a simple fast explicit integration method previously developed by Zhai [21], is employed. The scheme of this integration method is expressed as follows:

$$\begin{cases} \mathbf{X}_{n+1} = \mathbf{X}_n + \mathbf{V}_n \Delta t + (1/2 + \alpha)\mathbf{A}_n \Delta t^2 - \alpha \mathbf{A}_{n-1} \Delta t^2 \\ \mathbf{V}_{n+1} = \mathbf{V}_n + (1 + \beta)\mathbf{A}_n \Delta t - \beta \mathbf{A}_{n-1} \Delta t \end{cases} \tag{4}$$

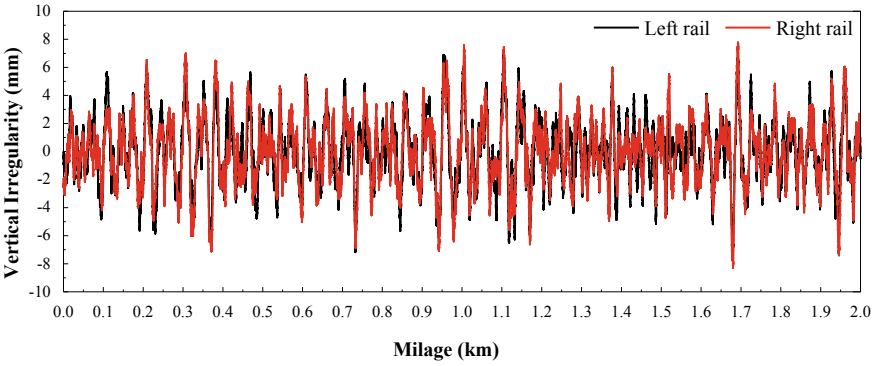

Fig. 3 Vertical random track irregularity

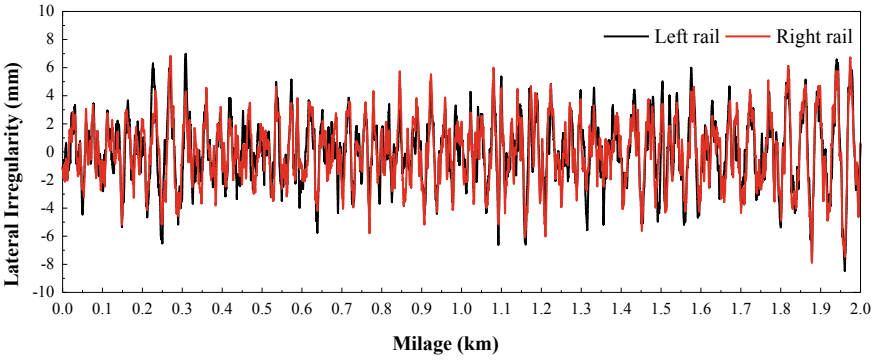

Fig. 4 Lateral random track irregularity

where **X**, **V** and **A** are the generalized displacement, velocity and acceleration of the system, respectively; Δt is the time step; the subscripts $n + 1$, n and $n - 1$ denote the integration time at $(n + 1)\ \Delta t$, $n\Delta t$ and $(n - 1)\Delta t$, respectively; α and β are free parameters that control the stability and numerical dissipation of the algorithm. Usually, a value of 0.5 could be assigned to α and β to achieve good compatibility between numerical stability and accuracy.

2.2 FE Model of Track–Tunnel–Soil–Building Subsystem

The geometric construction of the hotel and the tunnel is very complicated, as depicted in Fig. 1, and plays a key role in the vibration prediction of the hotel. The finite element method has the ability to elaborately describe their geometric construction, which is difficult to establish the dynamics model through analytical and semi-analytical methods. In order to predict the vibration of the hotel induced by moving train as accurate as possible, a FE model of track–tunnel–soil–building system is established, as shown in Fig. 5.

In reality, the soil is the infinite half-space and the track length is also regarded as infinite. However, the volume of the soil has to be limited in the FE model and the wave will be, therefore, reflected at the boundary which is inconsistent with the practice. In order to mitigate the boundary effect, the artificial boundaries or the infinite elements should be adopted to encase the FE model. It is easy to implement the artificial boundaries in the FE model by modifying the material properties and fixing the outside nodes of the outermost elements. These boundaries and the modified outermost elements are referred to as consistent viscous-spring artificial boundaries and viscous-spring boundary elements [22]. The material properties of the viscous-spring boundary elements are as follows:

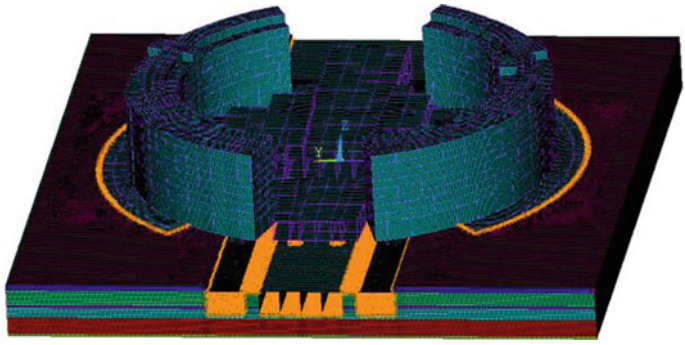

Fig. 5 General view of the FE model

Equivalent Poisson's ratio:

$$v' = \begin{cases} \frac{\alpha-2}{2(\alpha-1)}, & \alpha \geq 2 \\ 0, & \text{other} \end{cases} \tag{5}$$

Equivalent Young's modulus:

$$\mathrm{E}' = 2\alpha_T h \frac{G}{R}(1+v') \tag{6}$$

Equivalent damping ratio:

$$\eta' = \frac{\rho \mathrm{R}}{3G}\left(2\frac{v_\mathrm{s}}{\alpha_\mathrm{T}} + \frac{v_\mathrm{p}}{\alpha_\mathrm{N}}\right) \tag{7}$$

where $\alpha = \alpha_\mathrm{N}/\alpha_\mathrm{T}$, α_N and α_T are the parameters of the consistent viscous-spring artificial boundaries and generally equal to 4.0 and 2.0, respectively; ρ and G are the density and shear modulus of the soil; h and R are the thickness of the viscous-spring boundary element and the distance between the source of scattering wave and the consistent viscous-spring artificial boundary; v_p and v_s are the velocities of pressure wave and shear wave of the soil, respectively.

The damping of the embankment and the soil are also the key parameters for the attenuation of the wave propagation in the soil, so the damping parameters of the FE model should be set properly. In the material parameters, the density, elastic modulus, Poisson's ratio and damping have important influence on the ground vibration. The density, elastic modulus and Poisson's ratio can be directly defined; however, the Rayleigh damping is usually adopted in the FE method. The parameters of the Rayleigh damping are satisfied with

$$\begin{cases} \xi = \alpha/(2\omega_i) + \beta\omega_i/2 \\ \xi = \alpha/(2\omega_j) + \beta\omega_j/2 \end{cases} \tag{8}$$

where α and β are the parameters of the Rayleigh damping and relative with the mass and stiffness matrices, respectively; ξ is the damping ratio; ω_i and ω_j are the lower and upper limits of the range of predominant frequency range.

3 Numerical Prediction

3.1 Dynamics Parameters

The A-type metro train will be operated as planned. The train will be composed of six motor cars and two trailers as the head car and the tail car. The axle load of the train with normal passenger capacity is between 14 and 16 t. In order to attenuate

Table 2 Main dynamics parameters of the FST

Object	Parameter	Value	Object	Parameter	Value
Rail	Elastic modulus (MN/m^2)	210,000	Floating slabs	Length (m)	25
	Cross-sectional moment of inertia (m^4)	3.217×10^{-5}		Width (m)	4.2
	Density (kg/m^3)	7850		Thickness (m)	0.42
	Cross-sectional area (m^2)	7.745×10^{-3}		Density (kg/m^3)	2500
	Shear modulus (MN/m^2)	77,000		Elastic modulus (MN/m^2)	35,000
	Shear factor	0.4		Poisson's ratio	0.25
Fastener	Stiffness (MN/m)	30	Steel spring	Stiffness (MN/m)	6.6
	Damping (N s/m)	7.5×10^4		Damping (MN s/m)	4.9
	Fastener spacing (m)	0.595		Longitudinal spacing (m)	1.19

the building vibration induced by the moving train, a FST specially designed for this subway line is adopted. The natural frequency of the floating slab is about 8.2 Hz and the main dynamics parameters of the FST are listed in Table 2.

Before the construction of the hotel, a single-hole logging based on the geological prospecting method is generally adopted to investigate the shear wave velocity of the test field. In addition, the classical soil mechanic tests including the direct shear test and the three-axial test were applied to acquire the physical and mechanical parameters of the soil samplings from the in situ field. The test results provide important references to the dynamics properties of the in situ soil layers which are shown in Table 3. The main construction material of the tunnel and the building is reinforced concrete whose main dynamics parameters is well known and are not given here.

3.2 Predicted Results

The normal and the maximal operating speeds are planned as 80 km/h and 140 km/h. Firstly, the train–FST coupled dynamics model is used to calculate the fastener forces excited by the random track irregularities illustrated in Figs. 3 and 4 with the train

Table 3 Dynamics properties of the soil

Layer	Thickness (m)	Density (kg/m^3)	Young's modulus (MPa)	Poisson's ratio	Damping ratio
(1)	2.0	1.75×10^3	85	0.404	0.05
(2)	7.5	2.0×10^3	96	0.395	0.05
(3)	3.8	2.15×10^3	1271	0.311	0.05
(4)	48.4	2.5×10^3	5096	0.295	0.05

speed of 80 km/h. All of the fastener forces have a similar time history and one of them is illustrated in Fig. 6. It can be found that the max value of the fastener forces is about 55 kN. Then, all fastener forces are taken as the external loads of the FE model of track–tunnel–soil–building system to predict the building vibration.

Due to that the structure of the hotel is almost symmetrical about the longitudinal middle section of the tunnel, only three locations on each floor in the building on the left (see Fig. 1) are selected to illustrate the vertical acceleration of the building. The locations on each floor are illustrated in Fig. 7. The train is moving on the left subway line (see Fig. 1) with the speed of 80 km/h. The predicted vertical vibration of the building at those locations is as shown Fig. 8. In the Fig. 8, '*Fn*' represents the *n*th floor and the red and pink dotted lines are 62 dB and 65 dB, respectively, which are the limited values for night time and day time regulated by the standard [23].

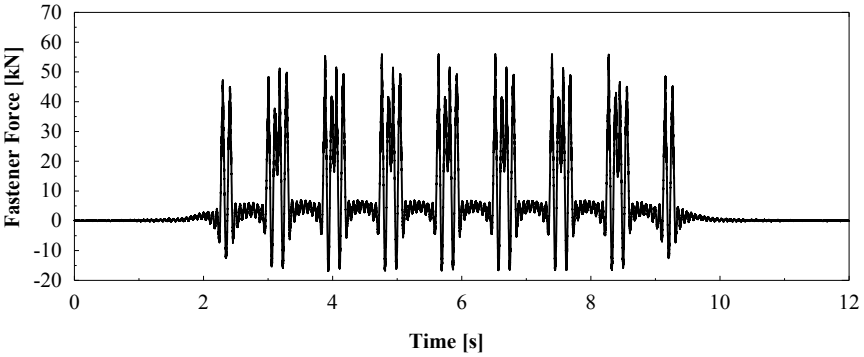

Fig. 6 Time histories of one fastener force

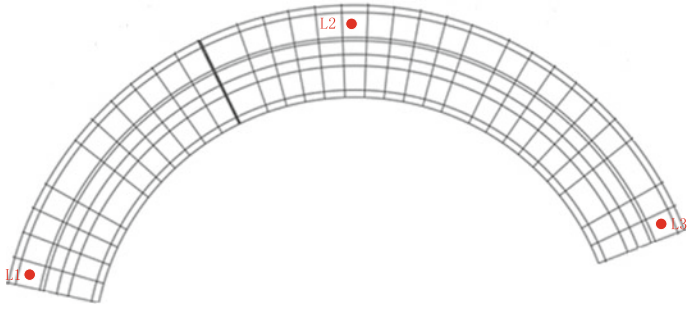

Fig. 7 Schematic diagrams of locations on each floor

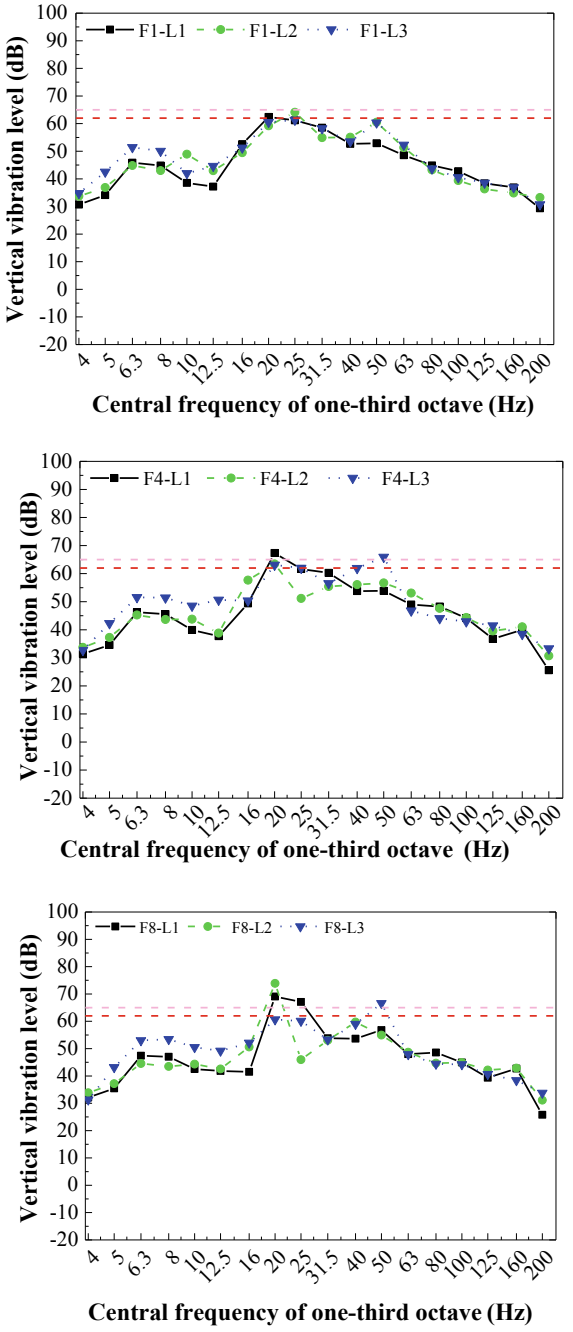

Fig. 8 Vertical vibration level of the building

It can be found from Fig. 8 that the vertical vibration of the building induced by the moving train is concentrated in the frequency range of 20 ~ 50 Hz. The first two dominant frequencies are close to the central frequency 20 Hz and 50 Hz, respectively. The vertical vibration level of those locations exceeds the limited values at those two dominant frequencies and the higher the floor is, the more the value exceeding the limit value is. so some vibration control measures have to be implemented. The vertical vibration level of the building also has a peak value in the frequency range of 6.3 ~ 8 Hz which probably induced by the natural frequency of the floating slab.

In order to evaluate the influence of train speed on the building vibration induced by the moving train, the comparisons are listed in Fig. 9. Compared to the results of the train speed 80 km/h, the building vibration induced by the moving train with speed of 140 km/h is smaller when the frequency is below the first dominant frequency and is larger when the frequency is above the second dominant frequency. This probably because the track vibration dominate the building vibration below the first dominant frequency and the wheel/rail forces dominates the building vibration above the second dominant frequency. When the train speed is 80 km/h, the wheelbase of the train is 2.5 m which will cause a characteristic frequency close

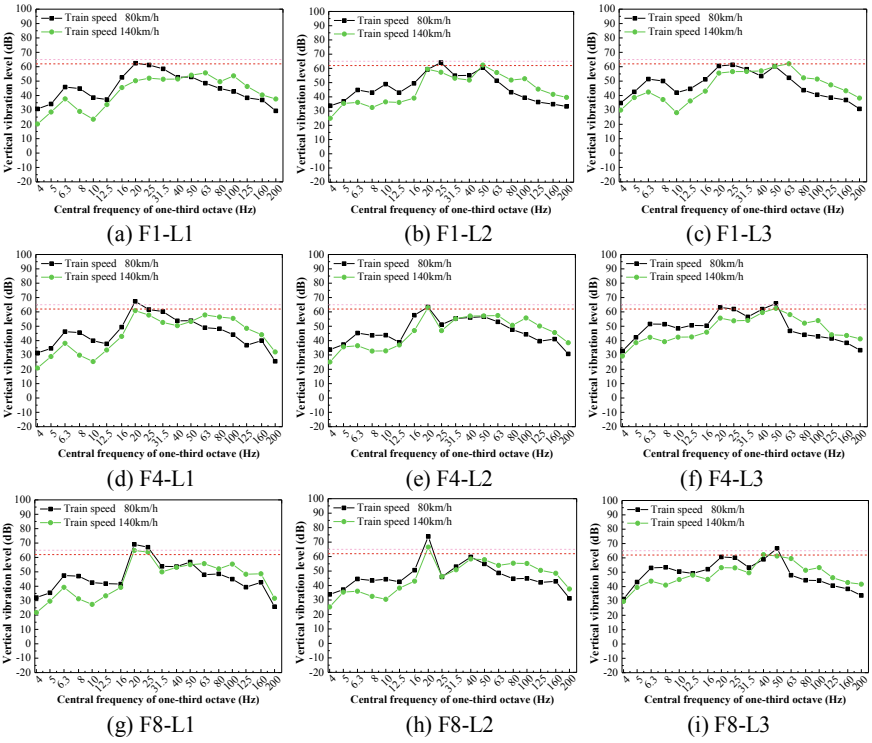

Fig. 9 Comparison of the vertical vibration level of the building induced by different train speed

to the natural frequency of the floating slab and the building vibration is aggravated below the first dominant frequency. When the train speed is 140 km/h, the dynamic wheel/rail interaction becomes more intensified and induces more aggravated building vibration above the second dominant frequency.

4 Conclusions

The vertical vibration of the building induced by the moving train is concentrated in the frequency range of 20 ~ 50 Hz. The first two dominant frequencies are close to the central frequency 20 Hz and 50 Hz, respectively. The vertical vibration level of those locations exceeds the limited values at those two dominant frequencies and the higher the floor is, the more the value exceeding the limit value is so some vibration control measures have to be implemented. Compared to the results of the train speed 80 km/h, the building vibration induced by the moving train with speed of 140 km/h is smaller when the frequency is below the first dominant frequency and is larger when the frequency is above the second dominant frequency.

Acknowledgements This work was supported by the National Natural Science Foundation of China (No. 11790283 and 51708457) and the Program of Introducing Talents of Discipline to Universities (111 Project) (Grant No. B16041).

References

1. Zhai W, Zhao C (2016) Frontiers and challenges of sciences and technologies in modern railway engineering. J Southwest Jiaotong University 51(2):209–226 (In Chinese)
2. Hunt HEM (1996) Modelling of rail vehicles and track for calculation of ground-vibration transmission into buildings. J Sound Vib 193(193):185–194
3. Balendra T., Koh, C. G., Ho., Y. C: Dynamic response of buildings due to trains in underground tunnels. Earthquake Eng Struct Dyn 20(3):275–291 (1991)
4. Bian X, Chen Y, Hu T (2008) Numerical simulation of high-speed train induced ground vibrations using 2.5D finite element approach. Sci China-Phys Mech Astron 51(6):632–650
5. Bian X, Jiang H, Chang C et al (2015) Track and ground vibrations generated by high-speed train running on ballastless railway with excitation of vertical track irregularities. Soil Dyn Earthq Eng 76:29–43
6. Yang Y, Hung H, Chang D (2003) Train-induced wave propagation in layered soils using finite/infinite element simulation. Soil Dyn Earthq Eng 23(4):263–278
7. Sheng X, Jones CJ, Thompson DJ et al (2005) Modelling ground vibration from railways using wavenumber finite- and boundary-element methods. Proc Roy Soc A Math, Phys Eng Sci 461(2059):2043–2070
8. Lombaert G, Degrande G (2009) Ground-borne vibration due to static and dynamic axle loads of intercity and high-speed trains. J Sound Vib 319(3):1036–1066
9. Forrest JA, Hunt HEM (2006) Ground vibration generated by trains in underground tunnels. J Sound Vib 294(4):706–736

10. Degrande G, Clouteau D, Othman R et al (2006) A numerical model for ground-borne vibrations from underground railway traffic based on a periodic finite element-boundary element formulation. J Sound Vib 293(3–5):645–666
11. Kouroussis G, Connolly DP, Verlinden O (2014) Railway-induced ground vibrations—a review of vehicle effects. Int J Rail Transp 2(2):69–110
12. Zhai W, Sun X (1994) A detailed model for investigating vertical interaction between railway vehicle and track. Veh Syst Dyn 23(sup1):603–615
13. Zhai W, Cai C, Guo S (1996) Coupling model of vertical and lateral vehicle/track interactions. Veh Syst Dyn 26(1):61–79
14. Zhai W, Wang K, Cai C (2009) Fundamentals of vehicle-track coupled dynamics. Veh Syst Dyn 47(11):1349–1376
15. Zhai W (2015) Vehicle-track coupled dynamics, vol 1, 4th edn. Science Press, Beijing. (in Chinese)
16. Chen G, Zhai W (2004) A new wheel/rail spatially dynamic coupling model and its verification. Veh Syst Dyn 41(4):301–322
17. Han H, Zhai W (2011) Numerical simulation of soft ground vibration caused by high-speed trains. advances in environmental vibration. In: 5th international symposium on environmental vibration. Science Press, Beijing, pp 142–150
18. Shao M, Zhai W, Song X et al (2013) Numerical simulation of high-speed train induced ground vibration for non-ballasted railway on embankment. In: 6th international symposium on environmental vibration. Science Press, Beijing, pp 3–14
19. Kouroussis G, Connolly D, Alexandrou G et al (2015) Railway ground vibrations induced by wheel and rail singular defects. Veh Syst Dyn 53(10):1500–1519
20. Chen G, Zhai W (1999) Numerical simulation of the stochastic process of railway track irregularities. J Southwest Jiaotong Univ 34(2):138–142 (in Chinese)
21. Zhai W (1996) Two simple fast integration methods for large-scale dynamic problems in engineering. Int J Numer Meth Eng 39(24):4199–4214
22. Liu J, Gu Y, Du Y (2006) Consistent viscous-spring artificial boundaries and viscous-spring boundary elements. Chin J Geotech Eng 28(9):1070–1075
23. JGJ/T 170–2009 (2009) Standard for limit and measuring method of building vibration and secondary noise caused by urban rail transit